Research Square

Preprints are preliminary reports that have not undergone peer review.
They should not be considered conclusive, used to inform clinical practice,
or referenced by the media as validated information.

Building blocks for 3D fuelbeds: object-centered scanning and meshing protocol

Iris Mire

imire@uw.edu

University of Washington School of Environmental and Forest Sciences

Jessie Thoreson

University of Washington School of Environmental and Forest Sciences

Susan Prichard

University of Washington School of Environmental and Forest Sciences

Michael Gallagher

USDA Forest Service Northern Research Station

Matthew Patterson

USDA Forest Service Northern Research Station

Nicholas Skowronski

USDA Forest Service Washington Office

Short Report

Keywords: Wildland fuels, digital twins, particle density, surface area-to-volume ratios

Posted Date: July 8th, 2026

DOI: https://doi.org/10.21203/rs.3.rs-9612145/v1

License: This work is licensed under a Creative Commons Attribution 4.0 International License.
Read Full License

Additional Declarations: No competing interests reported.

Version of Record: A version of this preprint was published at Fire Ecology on October 2nd, 2026. See the published version at https://doi.org/10.1186/s42408-026-00573-6.

Abstract

Background

Accurate modeling of wildland fuelbeds requires knowledge of not only where fuels are in three-dimensional (3D) space but also what they are. In this study, we introduce an object-based scanning protocol designed to generate detailed three-dimensional mesh models of individual fuel particles (e.g., seedlings, shrubs, litter, and cones) using an industrial-grade laser scanner. While traditional terrestrial laser scanning (TLS) or photogrammetric approaches tend to require objects to be segmented from broader-scope environment-level point clouds, our approach begins with the object itself.

Results

By scanning discrete plant parts in controlled conditions and capturing their morphology, surface area, and volume at sub-millimeter precision, we create a methodological foundation for fuel characterization that is structurally explicit and ecologically specific. We also propose a flexible workflow to adapt the scanning process for the extensive natural range of variation in fuel object structures, classifying individual objects based on their structural complexity.

Conclusions

Digital twins of wildland fuel plants and particles serve as building blocks for future integration with machine learning techniques to improve wildland fuelbed classification and simulation. Our approach shifts the basis of 3D fuels modeling from environmental scanning toward object-driven understanding with implications for fire behavior, emissions, and ecological modeling.

Introduction

Remote sensing technologies have revolutionized how forest structures are measured and monitored. Airborne laser scanning (ALS) and spaceborne lidar platforms have enabled large-scale characterization of canopy structure, providing datasets on tree height, crown shape, and overstory biomass with increasing spatial and temporal coverage (Arroyo et al., 2008; Bright et al., 2022; García et al., 2012; Skowronski et al., 2014). These technologies have greatly expanded the spatial reach of forest inventories and structure-based forest assessments (Kane et al., 2010; Lefsky et al., 2002; Næsset, 2004). However, they remain limited in their ability to adequately characterize surface fuel complexes in forest understories, shrublands, and grasslands—primarily due to occlusion from the canopy and the coarse resolution of most returns (Hamraz et al., 2017). Wildland fuelbeds are defined as complexes of fuels that are available to burn in a wildland fire event; these can include organic soils, litter, downed wood, herbaceous vegetation, shrubs, and tree crowns (Ottmar et al., 2007).

For wildland fire modeling, understanding the vertical and horizontal distribution of fuelbeds is essential—not just in forest canopies, but also in forest understories and at the forest floor, where fire ignition, spread, and intensity are often governed (Hiers et al., 2020; Loudermilk et al., 2022). Three-dimensional (3D) fire behavior and smoke models such as QUIC-Fire represent a major advance in mechanistic simulation but depend on gridded, 3D fuel inputs (Linn et al., 2020; Marcozzi et al., 2025). At present, these inputs are often derived from 2D datasets such as LANDFIRE, which provide generalized fuel classifications and canopy height layers but do not adequately capture the complexity or spatial arrangement of surface and understory fuels (Hyde et al., 2015; Krasnow et al., 2009). Vertical height alone is a poor proxy for key attributes such as bulk density, fuel type, or fine-scale connectivity—parameters that fundamentally influence flame dynamics and fireline intensity (Finney et al., 2021; Keane, 2015).

Terrestrial laser scanning (TLS) provides greater detail than ALS and addresses issues of canopy occlusion with ground-based 3D scans of forest plots that more accurately capture understory fuel presence and location (Calders et al., 2020). However, TLS still presents challenges for object identification and classification—especially at fine scales—and often cannot resolve or separate the structural intricacies of individual fuel elements such as grasses, litter, or small-diameter wood (Murphy et al., 2024). Consequently, TLS-derived metrics may correctly represent fuel height and location but still lack meaningful estimates of mass, fuel type, or combustion potential (Cova et al., 2023). Similarly, ALS and spaceborne systems are essential for capturing broad patterns of forest vegetation, but due to issues of canopy occlusion they cannot resolve forest understories with the granularity required for wildland fire modeling (Hiers et al., 2009; Loudermilk et al., 2012). Specifically, rapid advances are being made to support physics-based models of fire behavior and effects such as the Fire Dynamics Simulator (FDS) (Mell et al. 2007) and QUIC-Fire (Linn et al. 2021), which required gridded, 3D fuel inputs for canopy and surface fuels (e.g., Marcozzi et al. 2025). Because forest understories and other surface fuels are the primary target of most prescribed burning programs, modeling in support of prescribed burn decision support is particularly dependent on reliable characterization and mapping of understory fuels.

Here we introduce an object-based scanning protocol intended to complement coarser-scale remote sensing approaches. Instead of scanning complex wildland fuel environments (e.g., forest understories, shrublands, grasslands) in which fuels are interwoven and often occluded, we isolate and scan individual surface and fuel particles (e.g., seedlings, shrubs, litter, cones) (Keane, 2015) using a coordinate measuring machine (CMM): the FARO® Design ScanArm 2.5C (DSA) (FARO Technologies, Inc., 2019). This hybrid laser-contact system, originally developed for industrial metrology and reverse engineering (FARO Technologies, Inc. 2018), allows for sub-millimeter resolution scans of plant materials without deformation. FARO's RevEng software provides real-time visualization and enables cleaning, meshing, and metric analysis of the resulting point clouds (FARO Technologies, Inc., 2022).

By focusing on discrete fuel objects rather than complex fuelbeds, this method allows for standardized, high-fidelity measurements of surface area, volume, and morphology. The resulting point clouds are

converted into polygonal surface models known as meshes (Zhou et al., 2018). A mesh is a digital representation of an object surface, composed of a connected network of faces that approximate the object shape in 3D. Digital mesh models enable a range of geometric and physical analyses, such as estimating total surface area or enclosed volume, that are not readily available from point cloud data alone. We classify scanned objects by structural complexity and offer stepwise protocols to manage variation in shape, deformability, and occlusion. Meshed objects can be used for training data in machine learning pipelines, for physical analysis of fuel properties, or as modular components in simulated fuelbeds.

The objective of this case study was to generate 3D models of understory fuel objects using high-resolution laser scanning technology. The study was guided by two central questions: (1) Can scanning and meshing methods be developed to represent a range of relevant plants and plant parts common to prescribed burning programs? (2) How can meshed objects be used to measure key physical properties of wildland fuels including surface area, volume, particle density, and bulk density? We anticipate that this technological approach will be used to classify and estimate wildland fuels from point cloud measurements and construct simulated models of wildland fuel complexes.

Methods

Study Area

Samples including whole plants and plant parts were collected in and around Silas Little Experimental Forest in the New Jersey Pinelands, a UNESCO Biosphere Reserve (UNESCO, no date). Field sampling was conducted in late September 2024, and point cloud processing and mesh generation were completed in the following winter and spring. The collected seedlings, shrubs, ferns, downed wood, cones, and other understory fuels are representative species found in areas of the Pinelands managed with prescribed burns, which are conducted at Silas Little Experimental Forest and surrounding areas to reduce wildfire hazard and maintain and enhance fire adapted ecosystems. Sample locations, site attributes, and local conditions were recorded using ArcGIS Survey123 field app (ArcGIS Survey123 (field app), 2024), and in situ images were collected using a smartphone and Canon DSLR camera. Candidate species were selected based on consultation with local managers and ecologists in addition to relevant sites in the Digital Photo Series (Wright et al., 2010).

Objects were scanned with the DSA on site at Silas Little Experimental Forest within 48 hours of removal from the field (Fig. 1). After scanning, objects were labeled, packaged, and shipped to our Seattle, WA-based laboratory for drying and weighing. Samples were oven dried at 70 degrees Celsius for 48 hours (72 hours for coarse wood samples) to obtain dry weight biomass.

Scanning and Meshing Protocol

Our protocol is divided into scanning and meshing phases. The scanning phase encompasses all steps involved in generating and performing quality control on a point cloud, while the meshing phase focuses

on interpreting that point cloud as a 3D surface mesh composed of fine-resolution triangles. Given the wide variation in object size, configuration, and physical stability, the workflow has been tailored to accommodate the complexity of scanning and meshing each object. A streamlined workflow is applied to “simple” objects, such as individual leaves twigs, and needles, whereas a more detailed, nuanced approach is reserved for “compound” objects, such as shrubs and seedlings composed of leaves and stems. Specific adaptations of the protocol have been developed to address the form and context of real-world objects, including simple and compound objects.

Simple objects are composed entirely of a single 3D shape, typically cylindrical rod segments or flat planes. Examples include defoliated seedlings or shrubs with cylindrical branches (Fig. 2a) and planar leaves (Fig. 2b), represented by a single flat or slightly curved plane. Due to their consistent and predictable geometry, these objects are both straightforward to scan and process.

Compound objects are defined as composites of simple objects (i.e., a woody shrub with leaves) and can be processed most easily if first partitioned into its component parts. Several attributes may complicate the processing of these objects, including (1) self-occlusion (e.g., pinecone) (Fig. 3a); (2) composition involving multiple types of simple objects (e.g., foliated shrubs with both flat plane leaves and cylindrical stems) (Fig. 3b); (3) deformation potential due to movement (e.g., ferns, fresh leaves, palmetto fronds) (Fig. 3c).

Object preparation

To prepare for scanning, the turntable (FARO 8-Axis) was modified to enable secure attachment of the object to the axis surface. The method of attachment varied based on the object’s form and mass. Objects with stems or cylindrical bases (e.g., seedlings, downed wood) were attached using modeling clay or a clamp (Fig. 4). Objects without a cylindrical base (e.g., individual pinecones, some leaves) were secured at their base with modeling clay or foam. The goal was to maximize stabilization while minimizing occlusion from the laser line. Additionally, a square of 1/8-inch (0.3715 cm) foam mounting tape was placed around the center of the turntable to create stable tie points for post-scanning point cloud registration.

Prior to scanning, doors and windows were closed to minimize air flow and decrease the potential for noise and duplication in the point cloud due to object movement. To further limit turbulence around the scan, additional personnel remained stationary while scanning occurred. Additionally, a monitor with RevEng, was positioned to allow the person scanning to monitor scanning progress and quality in real time. After scanning, each sample was oven dried and weighed to the nearest 0.01 g.

Scanning protocol

To operate the DSA, the laser line probe was held between 45 and 90 degrees to the surface being scanned at a distance of approximately 15 cm. At the beginning of each scan, the base of the object (including the modeling clay and foam square) was scanned to ensure stable tie points in the final scan.

Next, the laser line was guided slowly along the surface until the point cloud shown on RevEng was sufficiently filled in. The probe was then rotated approximately 90 degrees, and the same section was scanned perpendicular to the initial swath, ensuring thorough coverage from multiple angles. The quality of the scan was periodically assessed, and areas that received poor coverage, or were missing in the initial scan, were rescanned. Each component of the object was scanned in this manner until sufficient point cloud coverage was achieved or all areas of the point cloud that could be filled in were captured. If the object was moved or otherwise deformed while scanning, the initial scan was discarded and scanning was repeated.

Compound objects are more challenging to capture than simple objects because they generally contain more areas of occlusion, can have complex leaf structure that is easily shifted or deformed by air flow in the scanning area, or are large and thus are challenging to reach all surfaces within the physical range limits of the scanner. Slight shifts in position led to duplication of some components in the point cloud, particularly with small diameter components including grass blades and pine needles. Similarly, objects with foliage and stems were challenging to scan because small branches and leaves created areas of occlusion that were impossible to scan without disturbing the position of the rest of the object.

Once each scan was completed (i.e., the point cloud in RevEng matched its real-world counterpart), the scan was paused for a cursory examination of scan quality. If missing areas were detected, scanning continued, focusing on the low-quality regions of the point cloud. If the scan appeared to be sufficiently detailed, the scan was saved. Before removing the object from the scan platform, a quality assessment of the point cloud was conducted in RevEng. Particular attention was focused on nodes, tie points, and small appendages (e.g., twigs). If the point cloud was missing elements of the object or contained low quality areas, then a supplementary scan was conducted. The supplementary scan followed the same process as the initial scan but with less comprehensive coverage, focusing solely on the low-quality areas. Scanning tie points and common features was critical to merging the separate scans together into one point cloud during post-processing.

The following aspects were considered in the assessment of point cloud quality: (1) **Occluded areas - a**ny areas that were occluded during the scan were identified and addressed with additional scans to ensure comprehensive coverage. In the case of compound objects, solving an occlusion issue could include defoliating the object and rescanning just the previously occluded branch architecture underneath. Specific issues that could not be addressed through additional scanning were documented and flagged for correction during point cloud processing or meshing. (2) **Nodes and complex, textured surfaces - s**pecial attention was paid to nodes (e.g., where a branch attaches to a stem or a leaf attaches to a branch) and complex, textured surfaces to ensure they were captured with sufficient point density and detail to accurately render the surface. (3) **Duplication - a**ny duplication of components in the point cloud was evaluated and corrected as necessary. Any limitations of the scanning process specific to the object, such as accessing areas that were occluded and could not be captured accurately were documented thoroughly to inform issues with point cloud processing and meshing.

Point cloud processing

Object point clouds are processed and prepared for meshing by manually cleaning the clouds, merging and co-registering the individual raw scans, and applying systematic outlier removal and smoothing algorithms. For this study, initial post-processing was conducted within RevEng (FARO Technologies, Inc., 2019). Objects with only one raw point cloud were manually cleaned by visually inspecting the point cloud and identifying areas with environmental noise or any points outside of the sample, including the clamp, clay, or foam anchoring the sample to the base of the 8-Axis. Points were removed using selection tools in RevEng. For objects with more than one raw point cloud, point cloud datasets were merged prior to cleaning. Once cleaned, point clouds were globally registered in RevEng to ensure global alignment, and normals of the point clouds were recomputed to ensure the proper orientation of all parts of the object. Any sections misoriented were noted and corrected in the mesh fixing stage. The registered point clouds were further cleaned by applying built-in "Outlier Removal" and "Smoothing" tools, which removed outlier points and smoothed the point cloud, respectively. The processed point cloud was then inspected for any features that might prove problematic for meshing, and any anomalies were documented. Thorough documentation at this stage was necessary to evaluate and record the quality of the mesh as a representation of the original point cloud.

Compared to simple objects, compound objects often contained more regions of occlusion that degraded fidelity to the real object. Processing the point cloud and documenting any low-quality areas while the object was still mounted on the scan platform was critical to accurately reconstruct missing elements. For example, where leaves were attached to stems in whorls, they were often heavily occluded. While nothing could be done to increase the quality of the scan directly, the targeted area could be photographed and noted for reference while generating and reconstructing the mesh in later steps.

Another relevant issue was the size of the point cloud (i.e., the number of points and the 3D space the point cloud occupied) and its impact on both processing time and scan quality. Because compound point clouds contained details that were necessary to scan and not easily interpolated by repair algorithms, they generally had more points than their simple counterparts of the same geometric size. While denser point clouds captured more of the nuance present in compound objects, they also slowed down every step of processing. Not only were they time consuming to process, they also could have quality issues due to small movements or general noise. The “Consolidate" tool was used on some of the noisier point clouds to eliminate duplicate points and filter the point cloud to a 0.1 mm resolution. The result was a thinned point cloud with approximately 60% of the number of points in the original and a much cleaner mesh.

Mesh generation

A mesh was generated from the processed point cloud. The “Generate” tool allowed the user to enable global alignment of point clouds, further thinning the point cloud to reduce noise, remove duplicate points, and improve point distribution through a grid filter option, with grid resolution set to 0.1 mm. The

resulting mesh was visually inspected to ensure that the mesh accurately reflected the point cloud. If all features were present and complete, then the mesh was deemed ready for mesh fixing. If some features were missing or showed substantial degradation from their analogs in the point cloud, then one or more of the following troubleshooting steps were taken. First, the mesh was regenerated using all points in the point cloud to provide more points for the mesh generation algorithm to tie to. Second, the mesh was regenerated using RevEng's recommended resolution for the point cloud (usually coarser than 0.1 mm). Missing or degraded elements were documented for fixing in the next stage.

Mesh fixing

Generated meshes were corrected using the "Repair" tool. All four Repair options in RevEng were selected. The Repair tool was run repeatedly until all small holes were filled. Each repaired mesh was overlaid with the original point cloud, and mesh quality was visually assessed to verify the presence or absence of all object components and surface coverage. The mesh that best visually represented the point cloud was selected for mesh finishing. After repairing the selected mesh, only large holes remained and were filled using the "Fill Holes" tool. Holes were filled manually, keeping as close to the boundaries of the point cloud as possible. The process continued until the mesh was fully closed (i.e., had no holes remaining).

Most compound objects could only be partially fixed in RevEng. The "Fill Holes" tool was effective and efficient at fixing cylinder segments and flat planes (i.e., simple objects), but ocular occlusion often obscured the target area and were degraded in mesh quality. Consequently, compound objects were best approached by splitting the original mesh into parts (i.e., stems versus individual leaves of a shrub or fern). Dividing the mesh into components allowed for more straightforward assessments of mesh quality and enabled the independent manipulation of object parts (Fig. 3d-f).

Metrics Calculations

For components that were easily made into continuous meshes (e.g., stems, coarse wood), the "Measure" tool in RevEng generated final surface area and volume values appropriate for further use. Surface area and volume were calculated for each component by using values generated by RevEng and geometric relationships (Fig. 5).

For meshes that were "one-sided" (e.g., objects so thin that the laser only recognized one side of the object such as leaves), RevEng calculated the surface area of only the scanned side of the object. Total surface area was calculated by multiplying the surface area value produced by RevEng by two. RevEng was also unable to calculate volume for one-sided meshes. To model the volume of these meshes, all were multiplied by a standard thickness value of 0.1 mm unless published thickness values were available.

The final surface area and volume were calculated using the following formulas:

$$\mathrm{SA}_{\mathrm{final}} = \mathrm{SA}_{\mathrm{RevEng}} \times 2 \quad \text{(Eq. 1)}$$

$$V_{final} = SA_{RevEng} \times T_{leaf}$$ (Eq. 2)

Where SA_{final} = two-sided surface area, SA_{RevEng} = one-sided surface area, V_{final} = calculated volume of one-sided mesh, T_{leaf} = published species leaf thickness value.

Results and Discussion

To date, 74 objects representing 10 fuel types and 23 species were sampled, scanned, and weighed from the case study area (Table 1). Once scanned, objects could be digitally parsed into their simple components (e.g., an oak seedling scan could yield individual point clouds for the intact object, leaves, and stem). Additionally, some objects were scanned twice to capture both foliated and defoliated states and to compensate for any occlusion of the stem in the foliated scan. Each object was also associated with a dry weight value in addition to descriptive attributes within a Survey123 form and Avenza waypoint, including imagery of the object in its natural state, geospatial location, scientific name, and object type (e.g., shrub, seedling, cone).

Table 1
Sample types, species names, and total record counts from the New Jersey Pinelands case study

Object Type	Species	Total Object Count
Graminoid	*Carex* sp. (sedge)	1
Forb	*Comptonia peregrina* (sweet fern), *Gaultheria procumbens* (American wintergreen), *Pteridium aquilinum* (bracken fern)	7
Shrub	*Gaylussacia baccata* (black huckleberry), *G. frondosa* (blue huckleberry), *Kalmia angustifolia* (sheep laurel), *K. latifolia* (mountain-laurel), *Lyonia mariana* (Piedmont staggerbush), *Quercus ilicifolia* (scrub oak), *Smilax glauca* (cat greenbrier), *Vaccinium pallidum* (Blue Ridge blueberry)	21
Seedling	*Pinus rigida* (pitch pine), *Pinus virginiana* (Virginia pine), *Q. alba* (white oak), *Q. coccinea* (scarlet oak), *Q. marilandica* (blackjack oak), *Q. montana* (chestnut oak), *Q.* stellata (post oak), *Q. velutina* (black oak), *Sassafras albidum* (sassafras)	19
Wood	*Q. montana* (chestnut oak)	3
Cone	*Pinus echinata* (shortleaf pine), *Pinus rigida* (pitch pine)	2
Leaf	*Q. alba* (white oak), *Q. coccinea* (scarlet oak), *Q. marilandica* (blackjack oak), *Q. montana* (chestnut oak), *Q. stellata* (post oak)	17
Litter	Mixed pine and oak litter	1
Vine	*Smilax rotundifolia (*roundleaf greenbrier)	1
Bark	*Pinus echinata* (shortleaf pine)	2

This protocol advances our ability to accurately and precisely render forests, shrublands, and grasslands in a digital twin environment that can be used to support precise measurements and also depict scanned vegetation in highly realistic, virtual environments. High-fidelity 3D models of understory fuels hold potential not only for forest management and decision support but also for the exploration of new digital frontiers in a multitude of disciplines and use cases. Digital twins are commonly used in engineering fields to render real world objects in 3D digital environments (Attaran and Celik, 2023), and digital twin environments are increasingly used to simulate real-word situations for learning and strategies for decision support such as emergency planning (Lagap and Ghaffarian, 2024), forensic investigations (Becker et al., 2025), and agricultural monitoring (Purcell and Neubauer, 2023). Highly realistic renderings of individual plants and fuel particles can be used to model fine-scale physical processes in which the precise form of individual objects is necessary to capture underlying mechanisms such as fine-scale fuel consumption and fire spread (Marcozzi et al., 2023). They may also be useful components of immersive virtual reality training tools for operational support.

By integrating high-resolution scans of fuel components into broader TLS or voxel frameworks, our methods offer a way to better parameterize 3D fire models with realistic, object-level detail. This technology allows us to collect discrete fuel elements—grasses, litter fragments, woody debris, and seedlings—as 3D objects to move beyond traditional voxel-based representations. Voxel grids are useful for partitioning space and estimating volumetrics, but they cannot readily represent the structural individuality of heterogeneous fuelbeds. An object-based approach enables direct measurement of attributes such as surface area, volume, packing ratio, and morphology. Additionally, instead of retroactively assigning physical fuel characteristics from lidar approaches, the CMM approach starts with fuel type and takes direct measurements of fuel particle properties. The structure, composition, and physical properties of objects can then inform voxelized attributes. We do not propose the DSA as a replacement for TLS or ALS, but rather as a complementary approach—one that enables a new level of ecological fidelity in fuel modeling. Together, these complementary tools can support the development of high-resolution, scalable fuel inventories necessary for accurate fire behavior prediction and decision support in fire-prone landscapes.

Potential limitations and implications for future studies

Although object scanning holds much promise for applications in ecology, including for fire and fuels modeling, there are several limitations to this approach. First, the DSA has a limited physical range both in terms of maneuverability and distance from the target surface. As such, it is not the best tool for extracting metrics for certain fuel types such as plants with dense outer leaf architecture. For some of the challenging objects within this study, the DSA point cloud could be used to create a visually accurate 3D rendering of object form but was not suitable for calculating surface area and volume without a high degree of error. Second, although the point clouds and meshes generated during this protocol can be exported from RevEng and edited in open-source software like CloudCompare (“CloudCompare,” 2024), the protocol is tailored to use of the DSA and RevEng, which are both costly and proprietary.

In RevEng, plane-based objects such as leaves or bark flakes cannot be easily represented by enclosed, watertight meshes. This issue mostly occurred when the thickness of the object was less than the minimum resolution of the DSA (0.1 mm). While the deviations from the true volume may only be on the order of millimeters, measurement errors could compound when modeled for all the leaves on a shrub or all the shrubs in a forest stand. To address this issue, subsequent studies could coordinate scanning with field measurements of leaf thickness to reduce uncertainty associated with calculated surface area and volume.

Future applications using this novel approach could explore ways to increase the efficiency and effectiveness of the scanning protocol and image processing. In this study, for example, some shrubs were only scanned with leaves still on the stems, which occluded much of the stem architecture. Branching architecture then had to be reconstructed from reference images, which introduced errors. In future work, the same shrub could be scanned twice, once with leaves on and again after being manually defoliated. Additionally, treating the stem and leaves separately and collecting dry weight biomass separately can allow objects to be attributed individually based on published particle density values, which are separated by fuel type (e.g., foliage, wood). Finally, we would recommend exploring more accessible methods to characterize wildland fuels in 3D. These could include laser-based, photo-based, and hybrid approaches. Based on the sheer variability of wildland fuels, a range of scanning and analytical approaches will be required.

Conclusions

This novel methodology for scanning wildland fuels represents a significant step toward achieving higher precision and accuracy in fuel particle and plant measurements. This study developed and evaluated methods to capture 3D architecture of plants and fuel particles. We also investigated how 3D meshes could be used to derive wildland fuel properties including surface area, volume, particle density, and bulk density. The 3D form of the fuel particle or entire plant not only yields the overall surface area and volume for the whole object but also allows for detailed investigation of where and how the surface area and volume are distributed throughout the object. Combined, the methods detailed in this study represent a major advancement in how wildland fuels can be measured and modeled in 3D.

Generating 3D digital twins of wildland fuels not only advances the precision and accuracy of complex measurements but also reveals new possibilities with applications in fire ecology and management. Specifically, the ability to create detailed 3D models of individual plants and fuel particles allows for the integration of these models into larger-scale simulations of planning units. By incorporating these detailed models into stand- or landscape-level analyses, researchers can develop a more realistic representation of wildland fuels, which can be translated into improved accuracy of inputs to models of wildland fire behavior and effects.

Declarations

Ethics approval and consent to participate: n/a

Consent for publication: n/a

Availability of data and material: The datasets and project metadata are being archived with Open Science Framework. Datasets are available upon request from the primary author.

Competing interests: The authors declare that they have no competing interests.

Funding: This research was funded by the Environmental Security Technology Certificate Program (ESTCP) and Strategic Environmental Research and Development Program (SERDP) through the FuelsCraft demonstration project (ESTCP RC23-7779). This research was supported (in part) by the U.S. Department of Agriculture, Forest Service. Any use of trade, firm, or product names is for descriptive purposes only and does not imply endorsement by the U.S. government.

Clinical trial number: not applicable

Author contributions: IM: conceptualization, data curation, formal analysis, investigation, methodology, validation, visualization, writing – original draft; **JT**: conceptualization, investigation, methodology, visualization, writing – review & editing; **SP**: conceptualization, funding acquisition, methodology, project administration, resources, supervision, validation, writing – review & editing; **NS**: conceptualization, methodology, resources, supervision, writing - review & editing; **MG & MP**: conceptualization, methodology, resources.

Acknowledgements: Thank you to Nicole Bendixen, Will Wall, Jacob Cook, and Kevin Brown for their essential field assistance at Silas Little Experimental Forest in the New Jersey Pinelands. Thank you to Barry Young and Ivan Barrow for DSA technical assistance.

References

1. ArcGIS Survey123 (field app), 2024.
2. Arkin, J., N. C. Coops, L. D. Daniels, and A. Plowright. 2023. Canopy and surface fuel estimations using RPAS and ground-based point clouds. *For Int J For Res*. https://doi.org/10.1093/forestry/cpad020
3. Arroyo, L. A., C. Pascual, and J. A. Manzanera. 2008. Fire models and methods to map fuel types: The role of remote sensing. *Forest Ecology And Management* 256:1239–1252. https://doi.org/10.1016/j.foreco.2008.06.048
4. Atchley, A. L., R. Linn, A. Jonko, C. Hoffman, J. D. Hyman, F. Pimont, C. Sieg, and R. S. Middleton. 2021. Effects of fuel spatial distribution on wildland fire behaviour. *Int J Wildland Fire* 30:179. https://doi.org/10.1071/WF20096
5. Attaran, M., and B. G. Celik. 2023. Digital Twin: Benefits, use cases, challenges, and opportunities. *Decis Anal J* 6:100165. https://doi.org/10.1016/j.dajour.2023.100165

6. Becker, S., T. H. Fritzsch, and D. Labudde. 2025. The role of a digital twin in supporting criminal investigations - a case report about a possible abuse. *Forensic Science, Medicine And Pathology* 21:245–254. https://doi.org/10.1007/s12024-024-00857-w
7. Bright, B. C., A. T. Hudak, T. R. McCarley, A. Spannuth, N. Sánchez-López, R. D. Ottmar, and A. J. Soja. 2022. Multitemporal lidar captures heterogeneity in fuel loads and consumption on the Kaibab Plateau. *Fire Ecol* 18:18. https://doi.org/10.1186/s42408-022-00142-7
8. Calders, K., J. Adams, J. Armston, H. Bartholomeus, S. Bauwens, L. P. Bentley, J. Chave, F. M. Danson, M. Demol, M. Disney, R. Gaulton, Krishna Moorthy, S. M. Levick, S. R. Saarinen, N. Schaaf, C. Stovall, A. Terryn, L. Wilkes, and P. Verbeeck, H. 2020. Terrestrial laser scanning in forest ecology: Expanding the horizon. *Remote Sensing Of Environment* 251:112102. https://doi.org/10.1016/j.rse.2020.112102
9. CloudCompare. 2024.
10. Cova, G. R., S. J. Prichard, E. Rowell, B. Drye, P. Eagle, M. C. Kennedy, and D. G. Nemens. 2023. Evaluating Close-Range Photogrammetry for 3D Understory Fuel Characterization and Biomass Prediction in Pine Forests. *Remote Sens* 15:4837. https://doi.org/10.3390/rs15194837
11. FARO Technologies, F. A. R. O. *Inc., 2022*. FARO RevEng.
12. FARO Technologies, FARO. ed. 2019. Inc., FARO® Design ScanArm User Manual.
13. Finney, M. A., S. S. McAllister, T. P. Grumstrup, and J. M. Forthofer. 2021. Wildland Fire Behaviour, 1st edition. ed. CSIRO Publishing.
14. García, M., S. Popescu, D. Riaño, K. Zhao, A. Neuenschwander, M. Agca, and E. Chuvieco. 2012. Characterization of canopy fuels using ICESat/GLAS data. *Remote Sensing Of Environment* 123:81–89. https://doi.org/10.1016/j.rse.2012.03.018
15. Hamraz, H., M. A. Contreras, and J. Zhang. 2017. Forest understory trees can be segmented accurately within sufficiently dense airborne laser scanning point clouds. *Scientific Reports* 7:6770. https://doi.org/10.1038/s41598-017-07200-0
16. Hiers, J. K., J. J. O'Brien, R. J. Mitchell, J. M. Grego, and E. L. Loudermilk. 2009. The wildland fuel cell concept: an approach to characterize fine-scale variation in fuels and fire in frequently burned longleaf pine forests. *Int J Wildland Fire* 18:315. https://doi.org/10.1071/WF08084
17. Hiers, J. K., J. J. O'Brien, J. M. Varner, B. W. Butler, M. Dickinson, J. Furman, M. Gallagher, D. Godwin, S. L. Goodrick, S. M. Hood, A. Hudak, L. N. Kobziar, R. Linn, E. L. Loudermilk, S. McCaffrey, K. Robertson, E. M. Rowell, N. Skowronski, A. C. Watts, and K. M. Yedinak. 2020. Prescribed fire science: the case for a refined research agenda. *FIRE Ecol* 16:11. https://doi.org/10.1186/s42408-020-0070-8
18. Hoffman, C. M., R. Linn, R. Parsons, C. Sieg, and J. Winterkamp. 2015. Modeling spatial and temporal dynamics of wind flow and potential fire behavior following a mountain pine beetle outbreak in a lodgepole pine forest. *Agricultural And Forest Meteorology* 204:79–93. https://doi.org/10.1016/j.agrformet.2015.01.018

19. Hyde, J., E. K. Strand, A. T. Hudak, and D. Hamilton. 2015. A Case Study Comparison of LANDFIRE Fuel Loading and Emissions Generation on a Mixed Conifer Forest in Northern Idaho, USA. *Fire Ecol* 11:108–127. https://doi.org/10.4996/fireecology.1103108
20. Kane, V. R., R. J. McGaughey, J. D. Bakker, R. F. Gersonde, J. A. Lutz, and J. F. Franklin. 2010. Comparisons between field- and LiDAR-based measures of stand structural complexity. *Canadian Journal Of Forest Research* 40:761–773. https://doi.org/10.1139/X10-024
21. Keane, R. E. 2015. *Wildland Fuel Fundamentals and Applications*. Cham: Springer International Publishing. https://doi.org/10.1007/978-3-319-09015-3
22. Krasnow, K., T. Schoennagel, and T. T. Veblen. 2009. Forest fuel mapping and evaluation of LANDFIRE fuel maps in Boulder County, Colorado, USA. *Forest Ecology And Management* 257:1603–1612. https://doi.org/10.1016/j.foreco.2009.01.020
23. Labenski, P., M. Ewald, S. Schmidtlein, F. A. Heinsch, and F. E. Fassnacht. 2023. Quantifying surface fuels for fire modelling in temperate forests using airborne lidar and Sentinel-2: potential and limitations. *Remote Sensing Of Environment* 295:113711. https://doi.org/10.1016/j.rse.2023.113711
24. Lagap, U., and S. Ghaffarian. 2024. Digital post-disaster risk management twinning: A review and improved conceptual framework. *International Journal Of Disaster Risk Reduction : Ijdrr* 110:104629. https://doi.org/10.1016/j.ijdrr.2024.104629
25. Lefsky, M. A., W. B. Cohen, D. J. Harding, G. G. Parkers, S. A. Acker, and S. T. Gower. 2002. Lidar remote sensing of above-ground biomass in three biomes. *Global Ecology And Biogeography* 11:393–399.
26. Linn, R. R., S. L. Goodrick, S. Brambilla, M. J. Brown, R. S. Middleton, J. J. O'Brien, and J. K. Hiers. 2020. QUIC-fire: A fast-running simulation tool for prescribed fire planning. *Environmental Modelling And Software* 125:104616. https://doi.org/10.1016/j.envsoft.2019.104616
27. Loudermilk, E. L., J. J. O'Brien, S. L. Goodrick, R. R. Linn, N. S. Skowronski, and J. K. Hiers. 2022. Vegetation's influence on fire behavior goes beyond just being fuel. *Fire Ecol* 18. 9, s42408-022-00132–9. https://doi.org/10.1186/s42408-022-00132-9
28. Loudermilk, E. L., J. J. O'Brien, R. J. Mitchell, W. P. Cropper, J. K. Hiers, S. Grunwald, J. Grego, and J. C. Fernandez-Diaz. 2012. Linking complex forest fuel structure and fire behaviour at fine scales. *Int J Wildland Fire* 21:882. https://doi.org/10.1071/WF10116
29. Marcozzi, A., L. Wells, R. Parsons, E. Mueller, R. Linn, and J. K. Hiers. 2025. FastFuels: Advancing wildland fire modeling with high-resolution 3D fuel data and data assimilation. *Environmental Modelling And Software* 183:106214. https://doi.org/10.1016/j.envsoft.2024.106214
30. Marcozzi, A. A., J. V. Johnson, R. A. Parsons, S. J. Flanary, C. A. Seielstad, and J. Z. Downs. 2023. Application of LiDAR Derived Fuel Cells to Wildfire Modeling at Laboratory Scale. *Fire* 6:394. https://doi.org/10.3390/fire6100394
31. Murphy, M. C., E. L. Loudermilk, S. Pokswinski, B. Williams, E. Link, L. Lienesch, L. Douglas, N. Skowronski, M. Gallagher, A. Maxwell, G. Snitker, C. Hawley, D. Wallace, I. Payne, T. Yurkiewicz, A. J. Sanchez Meador, C. Anderson, J. M. Jackson, R. Parsons, M. Floca, I. Nealey, I. Altintas, J. K. Hiers,

and J. Wallace. 2024. *Terrestrial 3D Laser Scanning for Ecosystem and Fire Effects Monitoring (No. SRS-GTR-277)*. Asheville, NC: U.S. Department of Agriculture, Forest Service, Southern Research Station. https://doi.org/10.2737/SRS-GTR-277

32. Næsset, E. 2004. Practical large-scale forest stand inventory using a small-footprint airborne scanning laser. *Scandinavian Journal Of Forest Research* 19:164–179. https://doi.org/10.1080/02827580310019257
33. Ottmar, R. D., D. V. Sandberg, C. L. Riccardi, and S. J. Prichard. 2007. An overview of the fuel characteristic classification system: quantifying, classifying, and creating fuelbeds for resource planning. *Canadian Journal Of Forest Research* 37(37):2383–2393.
34. Pimont, F., J.-L. Dupuy, R. R. Linn, and S. Dupont. 2011. Impacts of tree canopy structure on wind flows and fire propagation simulated with FIRETEC. *Annals Of Forest Science* 68:523. https://doi.org/10.1007/s13595-011-0061-7
35. Purcell, W., and T. Neubauer. 2023. Digital Twins in Agriculture: A State-of-the-art review. *Smart Agric Technol* 3:100094. https://doi.org/10.1016/j.atech.2022.100094
36. Ritter, S. M., C. M. Hoffman, M. A. Battaglia, C. S. Stevens-Rumann, and W. E. Mell. 2020. Fine-scale fire patterns mediate forest structure in frequent-fire ecosystems. *Ecosphere* 11:e03177. https://doi.org/10.1002/ecs2.3177
37. Rowell, E. M., E. L. Loudermilk, C. Hawley, S. Pokswinski, C. Seielstad, Ll. Queen, J. J. O'Brien, A. T. Hudak, S. Goodrick, and J. K. Hiers. 2020. Coupling terrestrial laser scanning with 3D fuel biomass sampling for advancing wildland fuels characterization. *Forest Ecology And Management* 462:117945. https://doi.org/10.1016/j.foreco.2020.117945
38. Sánchez-López, N., A. T. Hudak, L. Boschetti, C. A. Silva, K. Robertson, E. L. Loudermilk, B. C. Bright, M. A. Callaham, and M. K. Taylor. 2023. A spatially explicit model of tree leaf litter accumulation in fire maintained longleaf pine forests of the southeastern US. *Ecological Modelling* 481:110369. https://doi.org/10.1016/j.ecolmodel.2023.110369
39. Skowronski, N. S., K. L. Clark, M. Gallagher, R. A. Birdsey, and J. L. Hom. 2014. Airborne laser scanner-assisted estimation of aboveground biomass change in a temperate oak–pine forest. *Remote Sensing Of Environment* 151:166–174.
40. UNESCO, no date. New Jersey Pinelands [WWW Document]. UNESCO. URL https://www.unesco.org/en/mab/new-jersey-pinelands (accessed 9.3.25).
41. Wright, C., P. C. Eagle, and D. L. Olson. 2010. A high-quality fuels database of photos and information. *Fire Manag Today Wash DC* 70:27–31.
42. Zhou, Q.-Y., J. Park, and V. Koltun. 2018. Open3D: A Modern Library for 3D Data Processing. https://doi.org/10.48550/arXiv.1801.09847

Figures

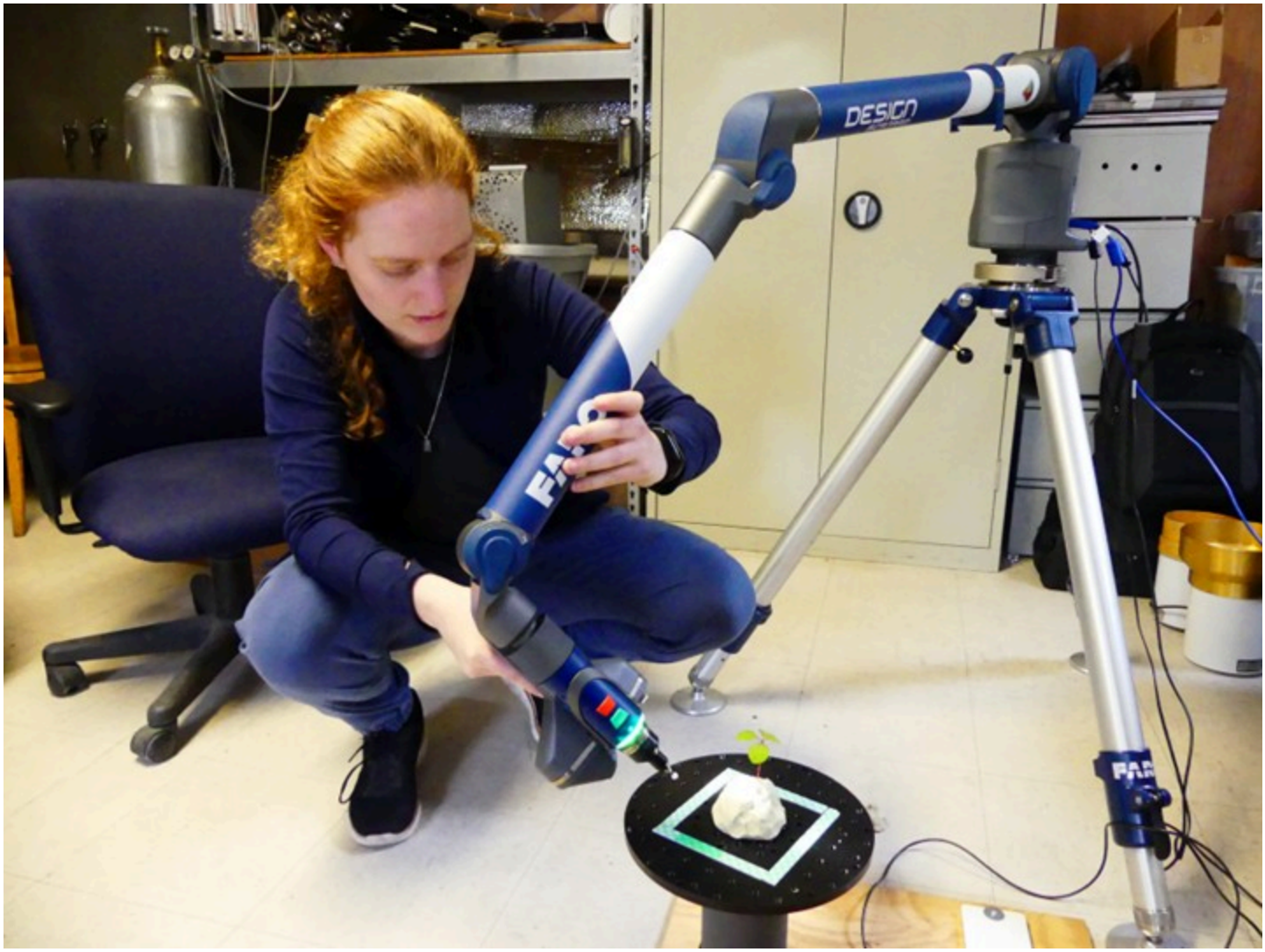


Figure 1

Scanning an individual plant, Eastern teaberry (*Gaultheria procumbens*).

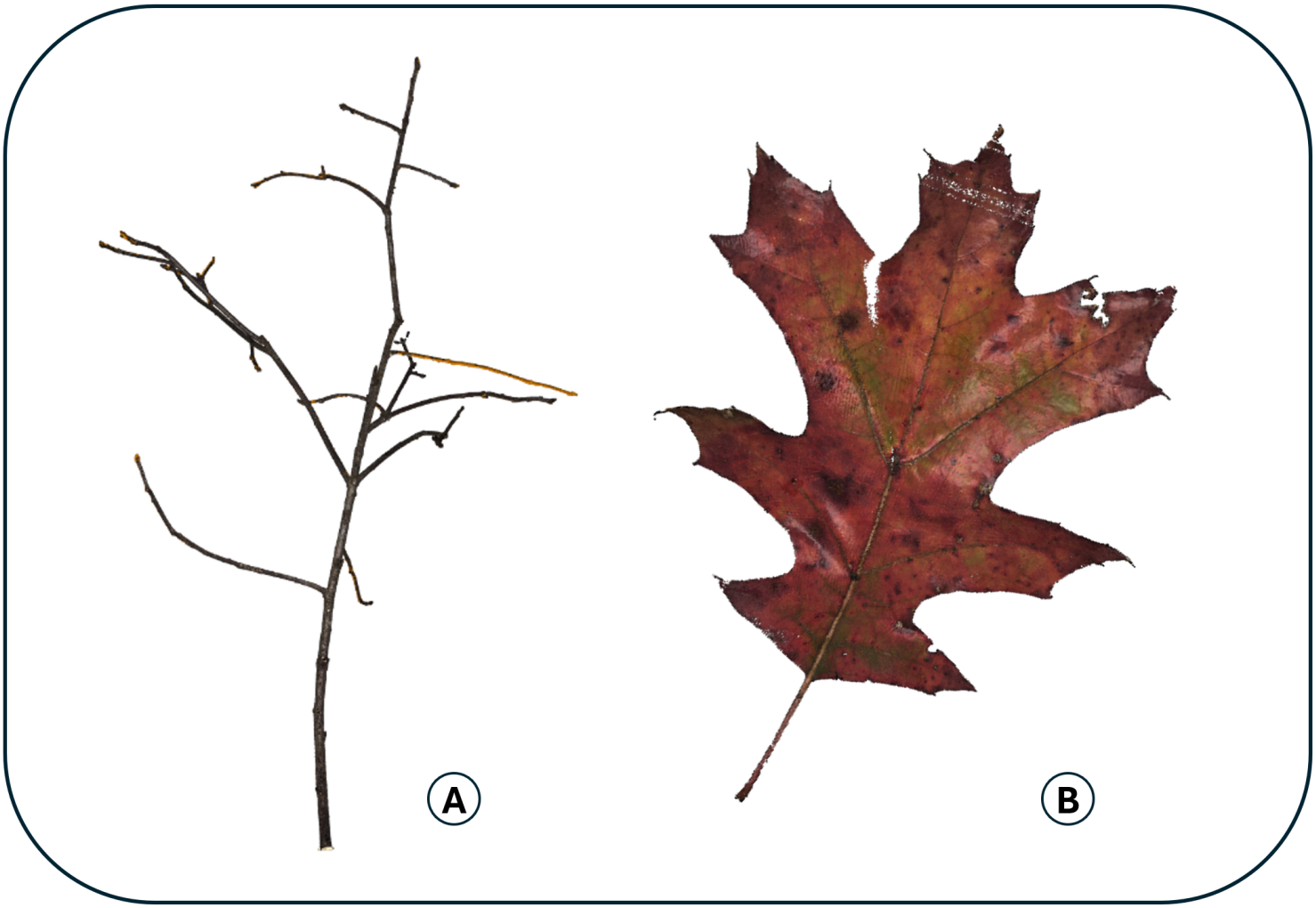


Figure 2

Raw DSA point cloud scans of two simple objects. A: defoliated black oak (*Quercus velutina*) seedling, B: scarlet oak (*Q. coccinea*) leaf.

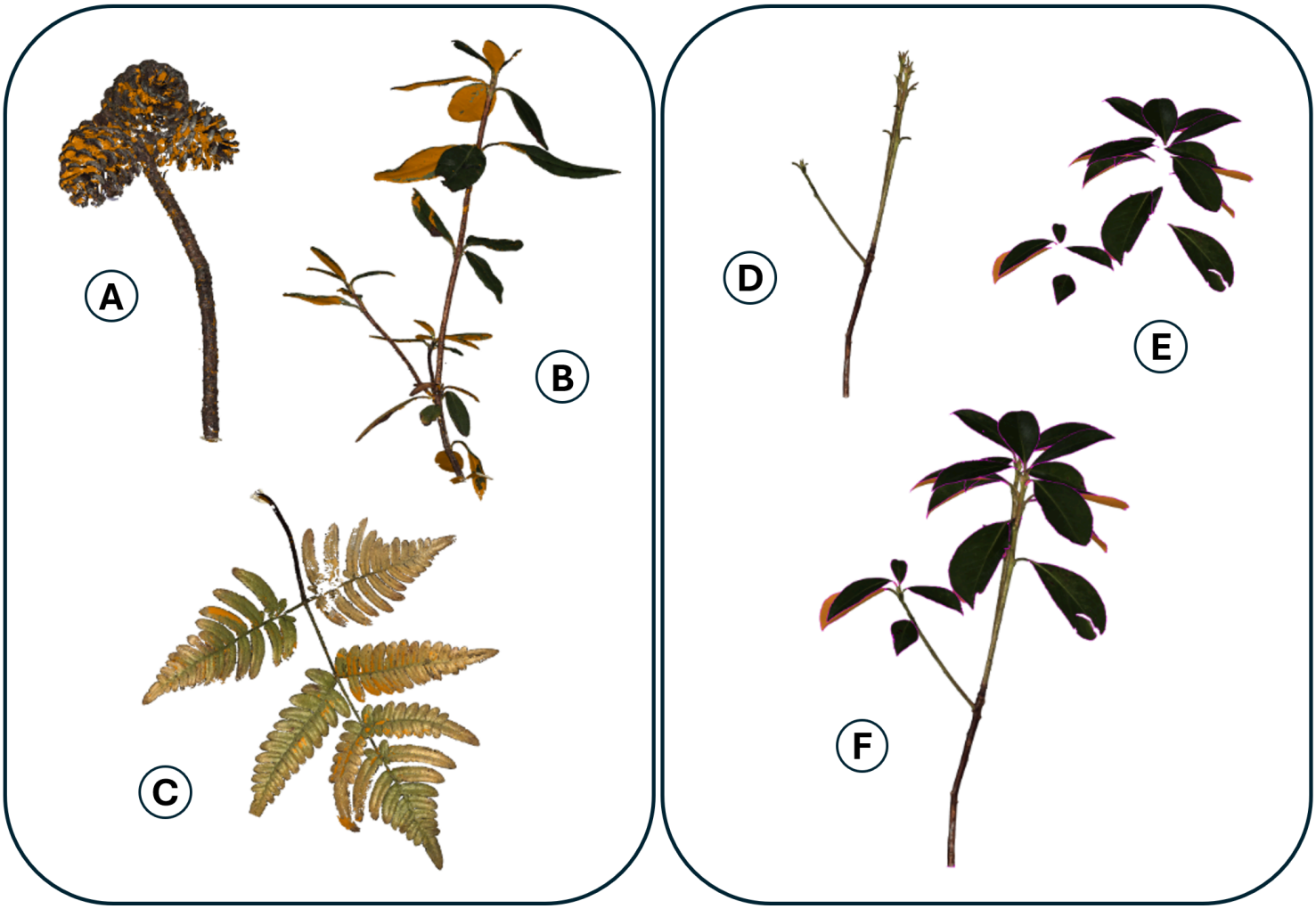


Figure 3

Compound object visualization. A: cones of shortleaf pine (*Pinus echinata*); B: sheep laurel (*Kalmia angustifolia*); C: bracken fern (*Pteridium aquilinum*); D: mountain-laurel (*K. latifolia*) stem–simple element of a compound sample; E: mountain laurel leaves–simple element of a compound sample; F: full mountain laurel sample–a combination of elements D and E.

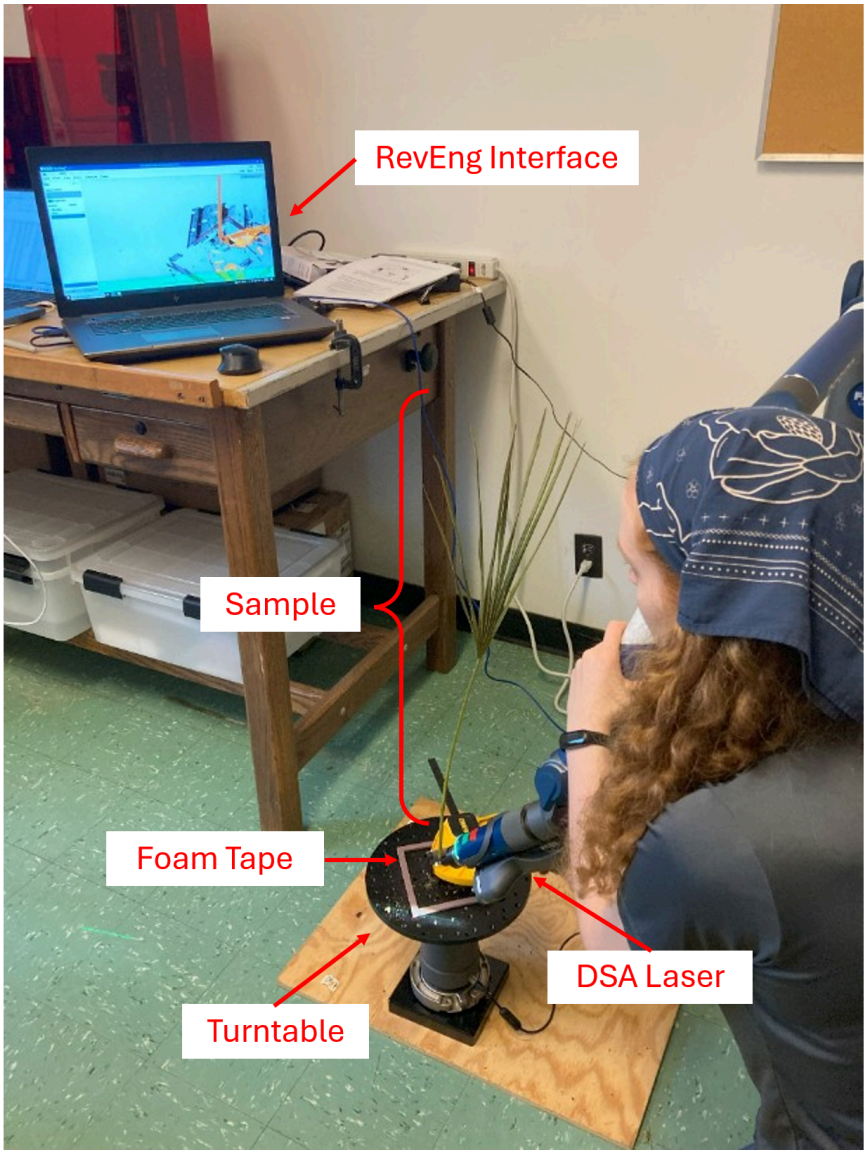


Figure 4

Example of scanning setup using the DSA, turntable, and RevEng software to scan a saw palmetto frond (Serenoa repens)

Description		Field Picture	Point Cloud	Mesh	Metrics
		A	B	C	D
Black Oak ***(Quercus velutina)*** **Type:** Simple **Sample ID:** NJP_AUT24_005	1				***Surface Area (mm²):*** *52578.016* ***Volume (mm³):*** *66300.703* ***Diagonal length (mm):*** *1208.045* ***Weight (g):*** *48.53*
White Oak ***(Quercus alba)*** **Type**: Simple **Sample ID**: NJP_AUT24_039	2	N/A			***Surface Area (mm²):*** *43881.574* ***Volume (mm³):*** *43881.574 x leaf thickness* ***Diagonal length (mm):*** *229.542* ***Weight (g)*** *1.58*
Mountain Laurel ***(Kalmia latifolia)*** **Type**: Complex **Sample ID**: NJP_AUT24_049	3				***Total Surface Area (mm²):*** *27904.115 (stem: 5554.549 + leaves 22189.305 one-sided)* ***Stem Volume (mm³):*** *3997.622* ***Leaf Volume (mm³):*** *22189.305 x leaf thickness* ***Diagonal length (mm):*** *398.951* ***Total Weight (g):*** *4.14 (stem: 1.99 + leaves: 2.15)*
Post Oak ***(Quercus stellata)*** **Type**: Complex **Sample ID**: NJP_AUT24_079	4				***Total Surface Area (mm²):*** *30546.877 (stem: 3750.988 + leaves: 26776.990 one-sided)* ***Stem Volume (mm³):*** *2548.833* ***Leaf Volume (mm³):*** *26776.990 x leaf thickness* ***Diagonal length (mm):*** *365.846* ***Total Weight (g):*** *4.19 (stem: 1.99 + leaves: 2.2)*

Figure 5

Sample comparison of field photos, point clouds, and meshes with metrics derived from the meshes, including surface area (mm^2), volume (mm^3), and diagonal length (mm). Sample dry weights (g) are provided. Leaf surface area and volume were calculated using Eq. 1 and Eq. 2, respectively.